Regularized Image Reconstruction for Ultrasound Attenuation Transmission Tomography

Igor PETERLÍK[1], *Radovan JIŘÍK*[1], *Nicole RUITER*[2], *Jiří JAN*[1]

[1] Dept. of Biomedical Engineering, Brno University of Technology, Kolejní 4, 612 00 Brno, Czech Republic
[2] Inst. for Data Proc. and Electr., FZ Karlsruhe, Hermann-von-Helmholtz Platz 1, 763 44 Eggenstein, Germany.

peterlik@ics.muni.cz, jirik@feec.vutbr.cz, Nicole.Ruiter@ipe.fzk.de, jan@feec.vutbr.cz

Abstract. *The paper is focused on ultrasonic transmission tomography as a potential medical imaging modality, namely for breast cancer diagnosis. Ultrasound attenuation coefficient is one of the tissue parameters which are related to the pathological tissue state. A technique to reconstruct images of attenuation distribution is presented. Furthermore, an alternative to the commonly used filtered backprojection or algebraic reconstruction techniques is proposed. It is based on regularization of the image reconstruction problem which imposes smoothness in the resulting images while preserving edges. The approach is analyzed on synthetic data sets. The results show that it stabilizes the image restoration by compensating for main sources of estimation errors in this imaging modality.*

Keywords

Ultrasound, transmission tomography, algebraic reconstruction techniques, regularization.

1. Introduction

Ultrasound transmission tomography is a potentially promising alternative to standard X-ray imaging in medical diagnosis, especially in mammography. This is mainly due to the non-ionizing character of ultrasound and high information content of the measured signals that could potentially result in high-resolution imaging.

The measurement setup is similar to the X-ray computed tomography setup [12]. The imaged object (e.g. human breast), immersed in a water tank, is surrounded by transducers emitting and receiving ultrasound field to and from various directions.

Compared to X-ray computed tomography, the ultrasound field and the image reconstruction algorithms are rather complex and computationally demanding. This is because the wavelength of ultrasound and the size of the imaged structures are comparable so that diffraction and refraction are substantial. As a result, ultrasound transmission tomography is still in the research state. More robust image restoration methods and application of more accurate mathematical models of the ultrasound field are needed.

Several ultrasound parameters of the tissue can be estimated. Reflectivity (echogenity) is the primary parameter utilized also in the conventional B-mode scanners. Further options for the imaged parameters are the speed of sound and the attenuation coefficient. Here, the ultrasound transmission tomography setup is considered with the aim to image a map of ultrasound attenuation-coefficient distribution in the immersed object. This tissue parameter is closely related to the tissue type and its pathological state and is thus of a high diagnostic value [6]. Hence, ultrasound attenuation tomography could be used as a standalone imaging modality. Furthermore, the obtained attenuation maps are intended to be used for correction in ultrasound reflectivity imaging [18], [5], which is a method utilizing the same signals with tissue reflectivity as the imaged parameter.

In the published methods [19], [11], [3], the principle is directly derived from X-ray computed tomography. The emitted ultrasonic pulse is supposed to propagate along a narrow straight line. Cumulative attenuation coefficients along the propagation paths are estimated and arranged to projections. The problem of attenuation-coefficient image reconstruction, formulated as the inverse Radon transform [12], may then be solved by means of the filtered backprojection method. The major artifacts of these methods are caused by refraction, phase cancellation (due to distorted phasefront of the received pulse or the non-normal incidence), varying speed of sound and pulse detection problems.

An alternative to the filtered backprojection are the so called algebraic reconstruction techniques (ART) [12]. The problem of an approximation to the inverse Radon transform is formulated as the solution of an overdetermined set of linear equations. This approach is more general because it can also be used for nonstraight propagation paths (e.g. reflected and scattered waves), which is potentially a valuable additional source of useful information [9].

Kaczmarz method of projections [12] is a well accepted ART method giving satisfactory results for problems with square matrices. The main advantage of the method is that it works only with one equation at a time and therefore, there is no need to load the entire system to the memory. Further, the method is convergent when the system matrix is invertible and no further assumptions about the system matrix are necessary unlike the other linear iterative methods. As the Kaczmarz method applied to overdetermined systems does not give optimal results (in the least squares sense), in [15], [16], an extended Kaczmarz method resulting in optimal least-squares solution is presented and applied in algebraic image reconstruction [17]. In [14] we have applied the extended Kaczmarz method to our problem of attenuation map reconstruction.

As the memory size and computational power is not a serious limitation in this context any more, the Kaczmarz methods can be replaced by more advanced solution techniques. In this paper, the use of regularization techniques [7], [2] is investigated which leads to a system of non-linear equations. The solution is again iterative, based on the half-quadratic algorithm presented in [4].

The contribution of this paper is the introduction of regularized image reconstruction techniques to the field of ultrasound transmission tomography. More specifically, an available edge-preserving regularization technique [2] was adopted to the restoration of attenuation-coefficient maps. This improves the solution of the equation set by including constraints on smoothness of the resulting attenuation-coefficient image while preserving edges (interfaces between the tissue structures). Using simulated data, the regularization method is analyzed with respect to the main sources of estimation errors in this modality.

2. Formulation of the Image Reconstruction Problem

The presented ultrasound attenuation tomography approach is derived for a two-dimensional (2D) setup, where the imaged object, immersed in a water tank, is enclosed by a ring of transducers (Fig. 1). At a time, one transducer is always in the emitting mode, while all other transducers record the received radiofrequency signals. Then, the next element is emitting and all remaining transducers are recording and so on, until all transducers have been used as emitters (see [20] for a description of such a 2D experimental transmission tomography system).

The emitted pulse is an undirected wave in the tomographic plane. Thus, the pulse spreads as a spherical wave; in the direction normal to the tomographic plane the pulse is supposed to be narrow. Such transmitted fields can be approximately achieved by a transducer with a small crossection in the tomographic plane and focused to this plane.

In this study, only the first pulse $s(t)$ of the received radiofrequency signal $rf(t)$ is used in the computation (see Fig. 1). It corresponds to the directly transmitted wave.

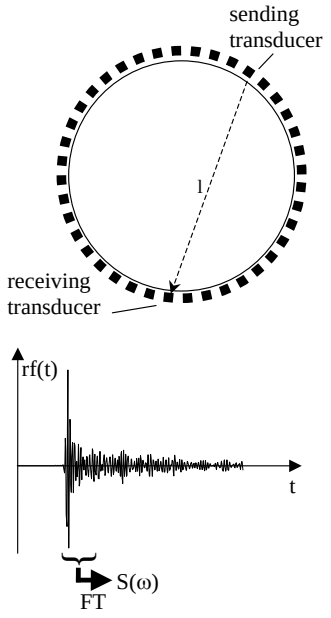

Fig. 1. Data acquisition in the 2D transmission tomography setup.

Taking any combination of the sending and receiving elements, the amplitude spectrum of the first-pulse signal $s(t)$ is [10]

$$|S(\omega)| = |S_0(\omega)| \cdot e^{-\beta d |\frac{\omega}{2\pi}|^n} \tag{1}$$

where ω is the frequency, d is the distance between the sending and receiving element and $S_0(\omega)$ is the spectrum of a pulse recorded with no object between the sending and receiving transducers (only water in the measurement tank, whereas the attenuation of water is neglected). It describes the electrical signal applied to the input of the sending transducer modified by the electroacoustical transfer functions of the transducers. β is the mean attenuation coefficient of the tissues along the direct propagation path l between the transducers, n is the frequency dependence coefficient of the attenuation; for soft tissues $n \approx 1$ [8].

Having a discretized attenuation-coefficient map in the tomographic plane, the mean attenuation coefficient β can be expressed using the local attenuation coefficients of each pixel β_i lying on the direct propagation path l:

$$\beta d = \sum_{i \in l} \beta_i d_i \tag{2}$$

where d_i is the length of the path l inside the i-th pixel. An overdetermined set of linear equations can be formulated based on (2) as

$$\mathbf{Rf} = \mathbf{p}. \tag{3}$$

Each equation corresponds to one combination of the sending and receiving transducers. The column vector of unknowns $\mathbf{f}$ consists of the local attenuation coefficients β_i of

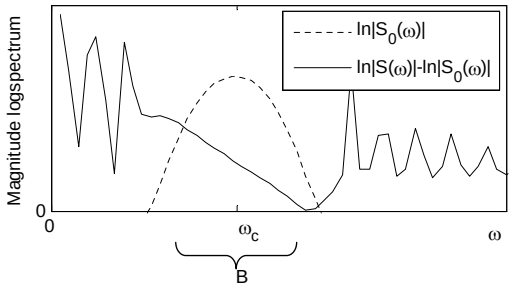

Fig. 2. Illustration of the logspectral difference method for estimation of the mean attenuation coefficient along a propagation path.

all pixels located inside the ring of transducers. The matrix R consists of pixel path-length values $d_{e,i}$, corresponding to d_i in (2), where i is the pixel index and e is the index of the equation, i.e. the propagation path. The right-side column vector $\mathbf{p}$ consists of the attenuation terms βd for each propagation path. It can be estimated by several methods [19]. Here, the logspectral-difference method is used. It is derived directly from (1) reformulated as

$$\beta d|\frac{\omega}{2\pi}|^n = \ln|S(\omega)| - \ln|S_0(\omega)|. \tag{4}$$

Hence, the logspectral difference on the right side of (4) is an approximately linear function of frequency for soft tissues. βd is estimated using linear regression as the slope of the logspectral difference, estimated in the frequency range corresponding to the transducer's bandwidth B (centered at the mean frequency ω_c of the transducers), see Fig. 2. As the method relies only on the shape of the logspectral-difference curve instead of energy levels of $S_0(\omega)$ and $S(\omega)$, it is more robust with respect to the refraction effects (which decrease energy of the wave detected at the receiving aperture) [19].

3. Regularized Image Reconstruction

3.1 Direct Image Reconstruction

The problem of attenuation-coefficient image reconstruction is formulated as a solution of the equation set (3). Let us assume that the number of available sender-receiver combinations is much higher than the number of unknown pixels in the resulting attenuation-coefficient image. Then, the system is overdetermined and there is no exact solution for the vector $\mathbf{f}$. Nevertheless, an optimal solution $\hat{\mathbf{f}}$ can be computed by minimization of a suitable functional $\mathcal{J}_1(\mathbf{f})$:

$$\hat{\mathbf{f}} = arg\min_{\mathbf{f}}(\mathcal{J}_1(\mathbf{f})). \tag{5}$$

The functional $\mathcal{J}_1(\mathbf{f})$ is based on the Euclidean norm as follows

$$\mathcal{J}_1(\mathbf{f}) = \frac{1}{2}\|\mathbf{p} - \mathbf{R}\mathbf{f}\|^2. \tag{6}$$

The necessary condition for a minimum of $\mathcal{J}_1$ is

$$\frac{\partial \mathcal{J}_1}{\partial f_i} = 0, \quad i = 1 \ldots n. \tag{7}$$

These equations are called *normal equations* and since the functional $\mathcal{J}$ is quadratic, the system (7) can be formulated as

$$\mathbf{R}^\top\mathbf{R}\mathbf{f} = \mathbf{R}^\top\mathbf{p}. \tag{8}$$

The system above is a linear $N \times N$ system that can be easily solved by some direct or iterative methods, e.g. LU decomposition.

3.2 Motivation for Regularization

The direct technique presented in the previous section gives reasonable results for accurate measurements of the mean attenuation coefficients forming the right hand side vector $\mathbf{p}$ and for a high degree of over-determination. However in practice, these assumptions are not valid and the quantitative attenuation-coefficient estimations are thus unsatisfactory [14]. The estimates of the mean attenuation coefficient along the propagation paths include many sources of errors:

- distortion of the wave front due to interference of time-delayed waves caused by diffraction and varying speed of sound in the imaged object,
- the transmission pulse and the scattered/reflected signals partially overlap in the received radiofrequency signal, causing errors in the transmission pulse determination,
- the positions of the senders and receivers are not given accurately,
- presence of noise in the measured radiofrequency signals.

Based on the assumed range of the mean attenuation coefficient, some equations can be detected as outliers and left out from the equation set. The lower bound of the mean attenuation coefficients is 0 (meaning positive coefficients), while the upper bound can be set according to the expected attenuation coefficients of the imaged tissue. Leaving out the outlier equations leads to a decreased degree of over-determination.

The right hand side vector of the remaining equations is degraded by the above listed errors. They can be modeled as an additive random noise term, in the first approximation.

To cope with the errors in the mean-attenuation-coefficient estimates, introduction of some additional information is needed, which would better constrain the desired solution. These constraints can be derived from the properties of the soft tissue. First, the tissue usually contains *homogeneous regions* with almost constant attenuation coefficient. Second, the imaged objects in the soft tissue (tumors or cysts) are assumed to have well-defined boundaries which

correspond to image *edges*—step changes in the attenuation coefficient.

This a priori information leads to two constraints:

(a) the homogeneous regions of the attenuation map should be smooth, i.e. the differences of neighboring pixels should be kept low

(b) the edges in the map should be preserved, i.e. the smoothing process should not blur the step changes of the attenuation coefficients

The above given constraints are frequently applied in the field of image deconvolution. Based on the problem formulation, these methods are known as regularized or Bayesian deconvolution [13]. Hence, a similar approach was applied to the problem at hand.

3.3 Edge-Preserving Regularization

One of the well known regularization techniques is the *Tikhonov regularization*. It is based on quadratic penalization of the differences between neighboring pixels [7]. However, this idea goes against one of our requirements which is the preservation of the important edges.

An improved technique, called *edge-preserving regularization* [2] seems to be suitable for the actual problem of the attenuation map reconstruction. It is based on minimization of an augmented functional

$$\mathbf{f} = arg\min_{\mathbf{f}}(\mathcal{J}_1(\mathbf{f}) + \lambda^2 \mathcal{J}_2(\mathbf{f})) \tag{9}$$

where J_2 is an additional regularizing term

$$\mathcal{J}_2(\mathbf{f}) = \sum_k \phi[(D_x f)_k/\delta] + \sum_k \phi[(D_y f)_k/\delta] \tag{10}$$

where $D_x f$ and $D_y f$ are differences between neighboring pixels (discrete image gradient components)

$$(D_x f)_{ij} = (f_{i,j+1} - f_{i,j}) \tag{11}$$
$$(D_y f)_{ij} = (f_{i+1,j} - f_{i,j}) \tag{12}$$

and both δ and λ are parameters defined bellow. The definition of the regularizing term shows that the differences $D_x f$ and $D_y f$ between neighboring pixels are again penalized. However, the penalization is given by a *potential function* ϕ which is an even cost function with specific properties enforcing the preservation of the edges.

In [2] three possible potential functions ϕ_{HS}, ϕ_{HL} and ϕ_{GM} are given. The plots of the functions are depicted in Fig. 3 and the mathematical definitions are:

$$\phi_{HS}(t) = 2\sqrt{1+t^2} - 2, \tag{13}$$
$$\phi_{HL}(t) = \log(1+t^2), \tag{14}$$
$$\phi_{GM}(t) = \frac{t^2}{1+t^2}. \tag{15}$$

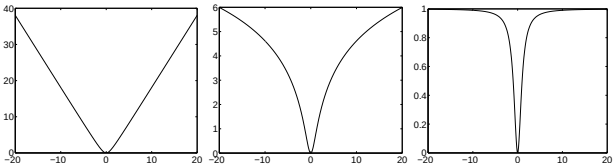

Fig. 3. Potential functions ϕ_{HS}, ϕ_{HL} and ϕ_{GM} from left to right. The first function ϕ_{HS} weakens penalization by calculating it as an approximation of a linear function, while both ϕ_{HL} and ϕ_{GM} slow down the penalization for large absolute values of the argument.

The first potential function ϕ_{HS} (an approximation of the absolute value) implements linear penalization of the differences between the neighboring pixels. Compared to the Tikhonov regularization (where the potential function ϕ was a quadratic function), high gradient values are penalized with a lower weight. However, the preservation of large gradients is not explicitly enforced.

The scenario is different when the potential functions ϕ_{HL} and ϕ_{HS} are considered. In both cases, for the small gradients, the penalization increases steeply with the gradient values, however it "slows down" as the differences $D_x f$, $D_y f$ further increase. This "slowing down" is more apparent in case of ϕ_{HS} when after some soft threshold the function is almost constant, i.e. with increasing difference, the penalization does not increase anymore.

The threshold is applied by multiplying the argument of the function by the parameter δ, see the definition of the regularizing term (10). Besides the parameter δ, there is another parameter λ which determines the weight of the term representing the regularization.

3.4 Half-Quadratic Optimization

Clearly, the functional containing the regularization term (10) is not quadratic. Therefore, the optimization becomes computationally expensive as the resulting system is non-linear.

In [2], [1] an algorithm based on *half-quadratic* minimization is described. The main idea behind the modification is to introduce auxiliary variables $\mathbf{b}_x$ and $\mathbf{b}_y$ and to derive an augmented functional $\mathcal{J}^*(\mathbf{f}, \mathbf{b})$ which has the same minimum in $\mathbf{f}$ as the original functional $\mathcal{J}_2(\mathbf{f})$, but it can be manipulated by linear algebraic methods [4]. The exact definition of the functional $\mathcal{J}^*(\mathbf{f}, \mathbf{b})$ can be found in [2].

The half-quadratic optimization is then performed as an iterative process where in (k)-th iteration two optimizations are executed as follows:

- having the actual estimation $\mathbf{f}^{(k)}$ fixed in, the functional $\mathcal{J}^*$ with respect to the auxiliary variable is minimized, i.e.

$$\mathbf{b}^{(k+1)} = arg\min_{\mathbf{b}} \mathcal{J}^*(\mathbf{f}^{(k)}, \mathbf{b});$$

- having the actual estimation of $\mathbf{b}^{(k+1)}$ fixed, $\mathcal{J}^*$ is minimized with respect to the original variable:

$$\mathbf{f}^{(k+1)} = arg \min_{\mathbf{f}} \mathcal{J}^*(\mathbf{f}, \mathbf{b}^{(k+1)}).$$

It can be shown that having fixed either the current estimate of $\mathbf{f}$ or $\mathbf{b}$, the augmented functional is quadratic in each argument and therefore each of the minimizations given above can be computed as a solution of a linear system of equations. The stopping criterium of the iterative process is defined as

$$\frac{\|\mathbf{f}^{(k+1)} - \mathbf{f}^{(k)}\|}{\|\mathbf{f}^{(k)}\|} < \epsilon \tag{16}$$

where ϵ is a constant related to the desired accuracy of the solution.

4. Results

4.1 Data and Evaluation

The algorithms were evaluated on simulated data, so that the estimated attenuation-coefficient map could be compared with the ground-truth map used for simulation. The simulation was designed to provide data corresponding to the experimental ultrasound transmission tomograph described in [20]. The ideal radiofrequency signals were generated assuming propagation of spherical waves with a constant sound speed. No diffraction and refraction effects were included. The test signals were generated for 100 equidistant transducer positions (a subset of transducers used in [20]). This leads to 100×100 sender-receiver combinations. Omitting the combinations where the sender and receiver are too close, the testing data set consisted of 7228 equations.

The resolution of the attenuation maps to be reconstructed was set to 50×50 pixels. Considering only pixels inside the transducer ring, this corresponds to 1256 unknowns.

The simulated attenuation map consisted of three disjoint homogeneous regions with different attenuation coefficients. Each of the regions had a sharp boundary represented by edges in the reconstructed image.

Having the reference attenuation map, the error of the reconstructed map was evaluated using the mean squared image difference e. Mathematically,

$$e = \frac{1}{MN} \sum_{m=1}^{M} \sum_{n=1}^{N} \left[f_{ref}(m,n) - \hat{f}(m,n) \right]^2 \tag{17}$$

where f_{ref} is the reference map, $\hat{f}$ is the reconstructed map and m, n are the spatial indices.

To analyze the importance of the regularization, two modifications of the simulated data were made. First, the right-hand side vector $\mathbf{p}$ of the system was distorted by additive Gaussian white noise in order to model the errors in the measurements of the mean attenuation coefficient along the propagation path, as described in section 3.2. The testing data sets with various *signal-to-noise ratio* (SNR) were created using different values of the noise variance.

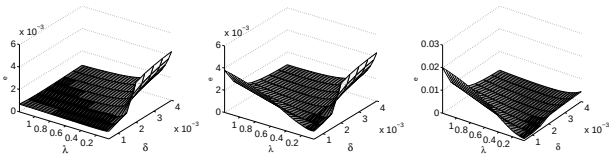

Fig. 4. Evaluation of the mean square differences as functions of the regularization parameters λ and δ. The plots are given for three data sets, each with a different noise level – SNR $= \infty, 11.3, 1.8$ from left to right. Potential function used: ϕ_{GM}.

For the second experiment, the system was reduced by omitting some equations. The reduced system contained only each n-th equation for $n = 2, 3, 4$. This was to model the case of omitting the equations with an out-of-range estimate of the mean attenuation coefficient.

4.2 Estimation of the Regularization Parameters

According to the definition given in (10) the regularization term contains two parameters δ and λ. The parameter values are not known a priori. Hence, the optimal parameter values for the data at hand were estimated first, i.e. parameters that give a minimal error e, defined by (17).

To analyze the regularization method with respect to the parameter values and to the right-hand-side degradation, the complete image reconstruction was applied to data sets with different SNRs and for a set of parameter values.

Having the particular data set, first some upper and lower limits for both parameters were set manually. Then, the intervals of interest for both parameters were divided into small steps and the reconstruction of the image was computed for each combination of the values. Fig. 4 shows the surface plots of the regularized-solution error (z axis) for varying λ and δ (x and y axis respectively). The plots are shown for various values of the SNR in the data set. For each case there is an "optimal valley" of minimal error. It turned out that the differences between the images obtained by regularization with parameters from the valley are basically negligible.

Altogether, it is important to perform a rough optimization of the parameters (mainly for the case with a higher level of noise), however it is sufficient to determine the optimal parameters approximately inside the valley. Furthermore, the study of the behavior of the regularization with respect to the parameters shows that the optimal values of the parameters differ for different level of the noise. This is as expected because higher error in the values of the right hand side needs a higher weight of the regularization term.

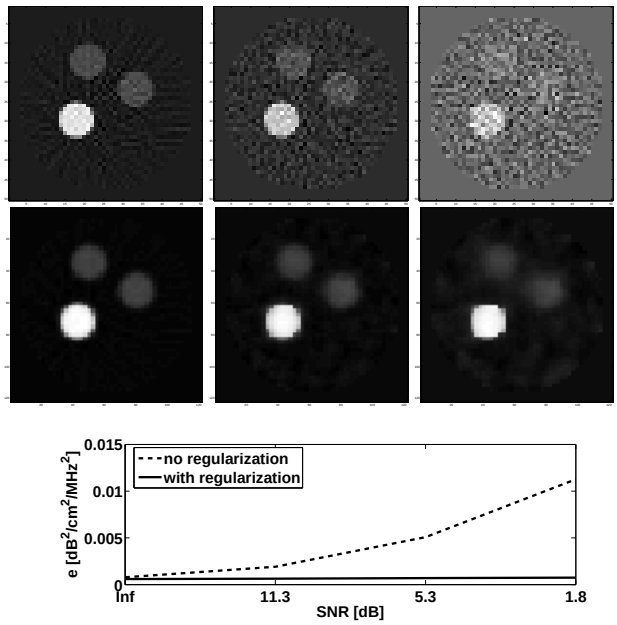

Fig. 5. The effect of the regularization for various SNRs. Non-regularized and regularized solutions in the first and the second rows, respectively, for SNR $= \infty$, SNR $= 11.3$ and SNR $= 1.8$ from left to right. The graph shows the comparison of mean squared errors for both methods quantitatively.

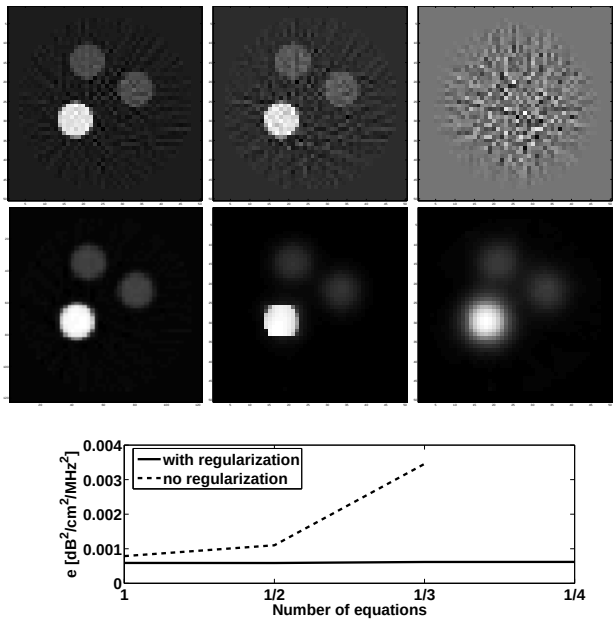

Fig. 6. The effect of the regularization on reduced equation systems. Non-regularized and regularized solution in the first and second row, respectively, for various numbers of the equations 7228 (full system), 2409 and 1807 equations from left to right. The graph shows the comparison of errors for both methods quantitatively. The error of non-regularized solution of system with 1807 is not shown as the system of the normal equations was singular.

The behavior of the parameters was very similar for all the potential functions ϕ_{HL}, ϕ_{HS} and ϕ_{GM}. However, the best results with the lowest norm of the error were achieved using the function ϕ_{GM}. This validates the approach based on the edge preservation as the map being reconstructed has three regions bounded by sharp edges and according to the reasons presented in section 3.3, the edges are best preserved by the potential function ϕ_{GM}.

4.3 Perturbed Right-Hand Side

In this section, the results concerning the regularization based reconstruction of the attenuation map from data with different SNRs are presented. The effect of the regularization is depicted in Fig. 5. In the case when the map is obtained just by the solution of the normal equations (8), the regions with different attenuation cannot be reliably resolved for SNR < 2. On the other hand, in the case when edge-preserving regularization (10) is applied, the objects are still well distinguished. The mean squared error increased with the noise level but to a much smaller extent than the non-regularized solution. Hence, it seems almost constant using the scale of Fig. 5. Both requirements from the section 3.2 are met as the homogeneous areas are clearly smoothed whereas the edges are still preserved. Moreover, further experiments showed that if the data are distorted with SNR < 1, the regions with different attenuation coefficient can be still distinguished, however, the edges become more blurred. Some artifacts similar to the real objects appear as well.

To summarize, the reconstruction from the data distorted by additive noise is significantly improved by the edge-preserving regularization. Naturally, there are some limits concerning the noise level.

4.4 Reduced Number of Equations

In this section, the behavior of the regularization for the system with a reduced number of equations is described. To obtain the results depicted in Fig. 6 the noise-free system was first used with all the equations, then reduced to one half, third and quarter of the original number of the equations, respectively.

The reduction of the number of the equations was tested on noise-free system. Therefore, the difference between regularized and non-regularized solution is negligible when all equations are used. The situation is similar also in the case, when a half of the equations is omitted. However, if only one third of the original number of the equations is considered, then the non-regularized system becomes singular and the corresponding image is therefore completely distorted whereas the regularized system is still solvable and the reconstructed image is reasonable. It turns out that even

if only one quarter of the original system is used, the regularized solution is still usable, albeit the edges become more blurred. The mean squared error increased with the smaller number of equations. Much steeper increase was observed for the non-regularized solution. Therefore, the regularized solution seems to give constant mean square error in Fig. 6 with the used scale.

According to the expectation, the regularization can help in the case when there is a lower number of equations available and the level of over-determination is lower.

5. Conclusion and Future Work

The paper presented use of regularized image reconstruction techniques in ultrasonic attenuation imaging by the transmission tomography setup. It can be seen as an alternative to the filtered backprojection or standard algebraic reconstruction techniques usually applied in this application field. The regularization stabilizes the image restoration by including some additional information in the solution. The analysis on simulated data showed that the suggested regularization could be used to compensate for errors in the mean attenuation measurements.

The main goal for the near future is to apply the reconstruction technique described in this paper to real data measured on phantom objects using the 2D and 3D experimental tomographs presented in [20] and [5]. The parameters of the regularization method will have to be adapted to the measured data. Application to the recorded data will also lead to a significant increase of the number of the equations (about 140 000 equations for the 2D system and about 3 500 000 equations for the 3D system) and therefore, advanced parallelization techniques will have to be considered.

The errors in the mean attenuation-coefficient estimates were modeled as a random additive variable. In the real measurement setup, this error depends, to a large extent, on the noise level in the recorded radiofrequency signal. This is, in turn, related to the emitting/receiving angle, due to the transducer angular characteristics. This means that the error in the mean attenuation-coefficient estimation is not completely random. Hence, the performance of the regularization technique might be slightly different on measured data compared to the simulated data.

The regularization technique was also tested on reduced equation sets, simulating the case when equations with the right-hand side outside of the expected range are excluded from the equation set. This was modeled by leaving out every n-th equation. For the recorded data, the pattern of the left-out equations will surely not be as regular as simulated here. The character will be partly stochastic (due to the measurement noise, imaged structures) and partly deterministic (depending on the emitting/receiving angle as mentioned in the previous paragraph). Hence, assessment of the regularization technique on the recorded data will have to be done in the follow-up work.

A drawback of the method that has to be studied further is the performance on data recorded from objects containing small structures. Depending on the regularization parameters (δ, λ), some small objects might be smoothed out.

The regularization can be further improved by considering a broader neighborhood of each pixel (not only the directly adjacent pixels). Depending on the properties of the uncertainties and noise, also some other types of constraints will be applied, e.g. the non-negativity as well as upper-bound constraints.

Acknowledgement

The project has been supported by the Czech Ministry of Education, Youth and Sports (Research Center DAR, proj. no. 1M6798555601) and the joint program of the German Academic Exchange Service and the Czech Academy of Science (grant. no. D12-CZ9/07-08), partly also by the research frame of the Czech Ministry of Education, Youth and Sports (grant no. CEZ MS 0021630513).

References

[1] CASANOVA, R., SILVA, A., AND BORGES, A. MIT image reconstruction based on edge-preserving regularization. *Physiological Measurements 25* (2004), 195–207.

[2] CHARBONNIER, P., BLANC-FERAUD, L., AUBERT, G., AND BARLAUD, M. Deterministic edge-preserving regularization in computed imaging. *IEEE Trans. Image Processing 6*, 2 (1997), 298–310.

[3] FITTING, D. W., CARSON, P. L., GIESEY, J. J., AND GROUNDS, P. M. A two-dimensional array receiver for reducing refraction artifacts in ultrasonic computed tomorgaphy of attenuation. *IEEE Trans. Ultrason. Ferroelec. Freq. Cont. UFFC-34*, 3 (1987), 346–356.

[4] GEMAN, D., AND YANG, C. Nonlinear image recovery with half-quadratic regularization. *IEEE Trans. Image Processing 4*, 7 (1995), 932–946.

[5] GEMMEKE, H., AND RUITER, N. 3D Ultrasound Computer Tomography for Medical Imaging. *Nuclear Instruments and Methods in Physics Research 580* (2007), 1057–1065.

[6] GREENLEAF, J. F., AND BAHN, R. C. Clinical imaging with transmissive ultrasonic computerized tomography. *IEEE Trans. Biomed. Eng.*, 28 (1981), 177 – 185.

[7] HANKE, M. Iterative regularization techniques in image reconstruction. In *Proceedings of the Conference Mathematical Methods in Inverse Problems for Partial Differential Equations* (1998), Springer-Verlag.

[8] HILL, C. R., BAMBER, J. C., AND TER HAAR, G. R. *Physical Principles of Medical Ultrasonics*. John Wiley & Sons, Inc., 2002.

[9] JIŘÍK, R., STOTZKA, R., AND TAXT, T. Ultrasonic attenuation tomography based on log-spectrum analysis. In *SPIE International Symposium on Medical Imaging, San Diego, USA* (2005), vol. 5750, pp. 305–314.

[10] JIŘÍK, R., TAXT, T., AND JAN, J. Ultrasound attenuation imaging. *Journal of Electrical Engineering 55*, 7–8 (2004), 180–187.

[11] KAK, A. C., AND DINES, K. A. Signal processing of broadband pulsed ultrasound: Measurement of attenuation of soft biological tissues. *IEEE Trans. Biomed. Eng. BME-25*, 4 (1978), 321–344.

[12] KAK, A. C., AND SLANEY, M. *Principles of Computerized Tomographic Imaging*. Society of Industrial and Applied Mathematics, 2001.

[13] LAGENDIJK, R. L., AND BIEMOND, J. *Iterative Identification and Restoration of Images (The International Series in Engineering and Computer Science)*. Springer, 1990.

[14] PETERLÍK, I., JIŘÍK, R., RUITER, N. V., STOTZKA, R., JAN, J., AND KOLAŘ, R. Algebraic reconstruction technique for ultrasound transmission tomography. In *Int. Conf. ITAB 2006* (Ioannina (Greece), 2006), pp. 6 pages, non–paginated.

[15] POPA, C. Least-squares solution of overdetermined inconsistent linear systems using Kaczmarz's relaxation. *Intern. J. Comp. Math. 55* (1995), 79–89.

[16] POPA, C. Extensions of block-projections methods with relaxation parameters to inconsistent and rank-deficient least-squares problems. *BIT Numerical Mathematics 38*, 1 (1998), 151–176.

[17] POPA, C., AND ZDUNEK, R. Kaczmarz extended algorithm for tomographic image reconstruction from limited-data. *Math. Comput. Simul. 65*, 6 (2004), 579–598.

[18] RUITER, N. V., SCHWARZENBERG, G. F., ZAPF, M., LIU, R., STOTZKA, R., AND GEMMEKE, H. 3D ultrasound computer tomography: Results with a clinical breast phantom. In *Ultrasonics Symposium, 2006. IEEE* (2006), pp. 989–992.

[19] SCHMITT, R. M., MEYER, C. R., CARSON, P. L., CHENEVERT, T. L., AND BLAND, P. H. Error reduction in through transmission tomography using large receiving arrays with phase-insensitive signal processing. *IEEE Trans. Sonics and Ultrasonics SU-31*, 4 (1984), 251–258.

[20] STOTZKA, R., WÜRFEL, J., AND MÜLLER, T. Medical imaging by ultrasound computertomography. In *SPIE's Internl. Symp. Medical Imaging 2002* (2002), pp. 110–119.

About Authors...

Igor PETERLÍK was born in 1981. He has a M.Sc. Degree (2004) in Informatics from Masaryk University, Brno. Currently, he is a PhD student at the Faculty of Informatics, Masaryk University as well as member of research team at the Department of Biomedical Engineering, Brno University of Technology. His research interests include numerical methods, parallel and distributed computing, medical simulations, soft tissue modeling and haptic interaction.

Radovan JIŘÍK was born in 1976. He has a M.Sc. degree (1999) in Cybernetics, Control and Measurement from the Brno University of Technology, Czech Republic. He has a Ph.D. degree (2004) in Biomedical Electronics and Biocybernetics from the Brno University of Technology, Czech Republic. Currently he is with the Department of Biomedical Engineering, Brno University of Technology as research and teaching assistant. His research interests include ultrasound imaging, image restoration, digital image and signal processing in biomedical engineering and modeling of biological systems.

Nicole V. RUITER was born in 1974. She has a M.Sc. degree (2000) in Medical Informatics from Ruprechts University Heidelberg, Germany. She has a Ph.D. degree (2003) in Informatics from the University of Mannheim, Germany. Currently she is with the Department of Data Processing and Electronics, Forschungszentrum Karlsruhe as scientist and head of the project Ultrasound Computer Tomography. Her research interests include ultrasound imaging, image reconstruction, digital image and signal processing and biomechanical models.

Jiří JAN was born 1941. He received his PhD degree in radioelectronics from the University of Technology, Brno (1969) and scientific degree I from the Czech Academy of Sciences, Prague (1986). He is currently Full Professor of Electronics as well as Head at the Department of Biomedical Engineering and Coordinator of the Institute for Signal and Image Processing, Faculty of Electrical Engineering and Communication, Brno University of Technology. His research interests include digital signal and image processing, including applications in biomedical engineering.